Mechano-Synthesis, Characterization, and Magnetic Properties of Nanoparticles of Cobalt Ferrite, $CoFe_2O_4$

Elina Manova,* Boris Kunev, Daniela Paneva, Ivan Mitov, Lachezar Petrov

Institute of Catalysis, Bulgarian Academy of Sciences, Acad. G. Bonchev Str., bl. 11, 1113 Sofia, Bulgaria

Claude Estournès,*,† Céline D'Orléans, and Jean-Luc Rehspringer

I.P.C.M.S. Groupe des Matériaux Inorganiques, UMR7504 CNRS, ULP, ECPM, 23 rue du Loess, BP 43, 67034 Strasbourg Cedex 2, France

Mohamedally Kurmoo

Laboratoire de Chimie de Coordination Organique, UMR7140, CNRS Université Louis Pasteur, Institut Le Bel, 4 rue Blaise Pascal, 67000 Strasbourg Cedex, France

Received May 21, 2004. Revised Manuscript Received September 17, 2004

Cobalt ferrite, $CoFe_2O_4$, nanoparticles have been obtained from pre-prepared layered double hydroxide carbonate, LDH-CO_3, by mechanical milling. X-ray powder diffraction shows the only product of the milling for 5 h of the LDH-CO_3 is cobalt ferrite nanoparticles. Longer-term milling induces particle growth characterized by sharpening of the Bragg peaks and an increase of the blocking temperature, while prolonged milling results in the formation of some cobalt metal. Mössbauer spectra and temperature dependence of the magnetization of the 5-h milled sample suggest that it consists of nanoparticles of size less than 10 nm with blocking temperature of 200 K, in good agreement with microscopy showing an average size of 6 nm. The magnetic properties exhibit a strong dependence on the particle size as a result of an unusual cation distribution and of surface effect. The saturation magnetization at 5 K and the squareness of the hysteresis loops increase with the average particle size. The difference between zero-field-cooled and field-cooled hysteresis loops is correlated with the presence of randomness of the moments at the surface.

Introduction

The synthesis of spinel ferrite nanoparticles has been intensively studied in recent years due to their potential application in high-density magnetic recording, microwave devices, and magnetic fluids.[1] It is well established that when the particle diameter is less than that of a single magnetic domain, spinel ferrite nanoparticles exhibit superparamagnetic properties, which is of great interest in macroscopic quantum tunneling between spin states.[2] Large-scale applications of ferrites of nanometer size and the tailoring of magnetic properties have prompted the development of several widely used methods, including sono-chemical reactions,[3] sol−gel techniques[4,5] reverse micelles,[6] host template,[7] coprecipitation,[8] microemulsion procedures[9] citrate precursor techniques,[10] microwave plasma,[11] and mechanical alloying,[12] for the fabrication of stoichiometric and chemically pure spinel ferrites nanoparticles. However, little is known about the use of mechanical milling in the preparation of ferrites from molecular precursors, in particular layered hydroxide compounds.

* Authors to whom correspondence should be addressed. Tel: +(359) 2 979 25 28. Fax: +(359) 971 29 67. E.M. e-mail: elina@ic.bas.bg. C.E. e-mail: claude.estournes@ipcms.u-strasbg.fr.

† Present address: Plate-forme Nationale de Frittage Flash, CIRIMAT, UMR5085 CNRS, Université Paul Sabatier, 118 route de Narbonne 31062 Toulouse Cedex 04, France. E-mail: estourne@chimie.ups-tlse.fr.

(1) Goldman, A. *Modern Ferrite Technology*; Van Nostrand Reinhold: New York, 1990. Berkovsky, B. M.; Medvedev, V. F.; Krakov, M. S. *Magnetic Fluids: Engineering Applications*; Oxford University Press: Oxford, 1993.

(2) Liu, C.; Zhou, B.; Rondinone, A. J.; Zhang, Z. J. *J. Am. Chem. Soc.* **2000**, *122*, 6263.

(3) Shafi, K. V. P. M.; Gedanken, A. *Chem. Mater.* **1998**, *10*, 3445.

(4) (a) Sugimoto, T.; Shimotsuma, Y.; Itoh, H. *Powder Technol.* **1998**, *196*, 85. (b) Kim, C. S.; Yi, Y. S. *J. Appl. Phys.* **1999**, *85*, 5223.

(5) Hutlova, A.; Nyznansky, D.; Rehspringer, J. L.; Estournès, C.; Kurmoo, M. *Adv. Mater.* **2003**, *15*, 1622.

(6) Seip, C. T.; Carpenter, E. E.; O'Connor, C. J. *IEEE Trans. Magn.* **1998**, *34*, 1111.

(7) (a) Kommareddi, N. S.; Tata, M.; John, V. T.; McPherson, G. L.; Herman, M. F. *Chem. Mater.* **1996**, *8*, 801. (b) Pham-Huu, C.; Keller, N.; Estournès, C.; Ehret, G.; Ledoux, M. J. *Chem. Commun.* **2002**, 1882. (c) Pham-Huu, C.; Keller, N.; Estournès, C.; Ehret, G.; Ledoux, M. J. *Phys. Chem. Chem. Phys.* **2003**, *5*, 3716. (d) Keller, N.; Pham-Huu, C.; Shiga, T.; Estournès, C.; Greneche, J.-M.; **2004**, *272-276*, 1642. Ledoux, M. J. *J. Magn. Magn. Mater.* Published on-line February 2, 2004. (e) Keller, N.; Pham-Huu, C.; Estournès, C.; Ehret, G.; Ledoux, M. J. *Carbon* **2004**, *42*, 1395.

(8) (a) Seki, M.; Sato, T.; Usui, S. *J. Appl. Phys.* **1988**, *63*, 1424. (b) Chen, Q.; Zhang, Z. J. *Appl. Phys. Lett.* **1998**, *73*, 3156. (c) Kim, Y. I.; Kim, D.; Lee, C. S. *Physica B* **2003**, *337*, 42.

(9) (a) Pillai, V.; Shah, D. O. *J. Magn. Magn. Mater.* **1996**, *163*, 24. (b) Lopez Perez, J. A.; Lopez Quintela, M. A.; Rivas, J.; Charles, S. W. *J. Phys. Chem. B* **1997**, *101*, 8045. (c) Feltin, N.; Pileni, M. P. *Langmuir* **1996**, *13*, 3927. (d) Moumen, N.; Veillet, P.; Pileni, M. P. *J. Magn. Magn. Mater.* **1995**, *149*, *67*.

(10) Prasad, S.; Gajbhiye, N. S. *J. Alloys Compd.* **1998**, *256*, 87.

(11) Hochepield, J. F.; Bonville, P.; Pileni, M. P. *J. Phys. Chem. B* **2000**, *104*, 905.

10.1021/cm049189u CCC: $27.50
Published on Web 11/25/2004

Mechanical milling of metal complexes with the precise amount of the required transition metals is a method with two advantages: (a) it can be easily operated and (b) it can produce large amounts of nanostructured powders in a fairly short time.[13] The high-energy milling as a solid-state processing method has been the subject of great interest in recent years.[14] Furthermore, the highly nonequilibrium nature of the milling process allows one to prepare solids with improved and/or novel physical and chemical properties.[15] The flexibility of the structure of spinel ferrites, $(M_{1-x}Fe_x)[M_xFe_{2-x}]O_4$, where M is a divalent metal ion, provides a wide range of physical behaviors and its preparation by mechanical milling is highly sought. Here, round and square brackets denote cation sites of tetrahedral (A) and octahedral [B] coordination, respectively. The value x in the general formula represents the degree of inversion (defined by the fraction of (A) sites occupied by Fe^{3+} cations). A mechano-chemical route for the preparation of ferrites has been reported[16] where the ferrite with the spinel structure was prepared from the oxides as starting materials. It has already been demonstrated to be an appropriate model system for such processing studies.[16a,17] Although extensive studies have been performed on the ferrites synthesized by high-energy ball milling from metal oxides, no synthesis, to the best of our knowledge, of cobalt ferrites has been reported by milling layered double hydroxides. It is well-known that LDH can be prepared by simple chemical precipitation and is an economical way to produce ultrafine powders as well as controllable metal content.[18] Here, we describe the application of a mechano-chemical technique for the synthesis of cobalt ferrite, $CoFe_2O_4$, from LDH-CO_3. We also present the characterization using powder X-ray diffraction, infrared spectroscopy, transmission electron microscopy, Mössbauer spectroscopy, and a study of the magnetic properties of samples prepared at different milling times.

Experimental Section

Materials and Synthesis of Percursor and Nanoparticles. The starting materials used were $Fe(NO_3)_3{\cdot}9H_2O$ (purity 99%), $Co(NO_3)_2{\cdot}6H_2O$ (purity 96%), and Na_2CO_3. Cobalt ferrite powders ($CoFe_2O_4$) were prepared in two steps: (1) coprecipitation to obtain the precursor, and (2) mechanical milling of the precursor. For the coprecipitation process, 0.5 M solutions of metal salts containing Co^{2+} and Fe^{3+} are taken in the desired molar ratio. The mixed cobalt and iron hydroxide carbonate precursor, $CoFe_2(OH)_4(CO_3)_2{\cdot}nH_2O$, is formed when a 1 M sodium carbonate solution is added until the pH = 9 under ultrasonic treatment. The initially formed precipitate was kept under continuous stirring and ultrasonic treatment for 1 h at room temperature (RT). After filtration, washing, and drying at RT, brown substances with layered structure are formed. The as-obtained precursor powders were milled using a Fritsch Planetary miller in a hardened steel vial together with fifteen grinding balls having different diameters (ranging from 3 to 10 mm). The ball-to-powder mass charge ratio was 6:1. The powders were milled for 5 h (sample denoted **MS5**), further milled for another 5 h (sample denoted **MS10**), and finally milled for 5 h with ball to powder mass charge ratio 12:1 (sample denoted **MS15**). The formation reaction is as follows:

$$CoFe_2(OH)_4(CO_3)_2{\cdot}nH_2O \Rightarrow CoFe_2O_4 + (2+n)H_2O + 2CO_2$$

Physical Techniques. The powder X-ray diffraction (XRD) patterns were recorded by use of a TUR M62 diffractometer with Co Kα radiation (λ = 1.789 Å). The observed patterns were cross-matched with those in the JCPDS database. The IR spectra were recorded by transmission through KBr pellets containing about 1% of the compounds by use of a FTIR ATI Mattson Genesis series spectrometer. Transmission electron microscopy (TEM) investigations were made using a Topcon 002B electron microscope operating at 200 kV with a point-to-point resolution r = 1.8 Å. The samples were sonicated in ethanol and deposited on a pre-deposited polymer on a copper grid. Mössbauer spectra of nanosize cobalt ferrite particles were recorded at 295 and 77 K on a Wissel electromechanical Mössbauer spectrometer (Wissenschaftliche Elektronik GmbH, Germany) working in a constant acceleration mode. A ^{57}Co/Cr (activity ≅ 10 mCi) source and an α-Fe standard were used. The experimental spectra were treated using the least-squares method. The parameters of hyperfine interaction such as isomer shift (IS), quadrupole splitting (QS), and effective internal magnetic field (H_{eff}), as well as the line widths (fwhm) and the relative weight (G) of the partial components of the spectra were determined. Temperature and field dependences of the magnetization of the cobalt ferrite were measured on a Quantum Design MPMS-XL SQUID operating in the temperature range 2−400 K and an applied field up to 5 T. To avoid sample rotation in the applied field the nanoparticles were embedded in a polymer matrix of poly methyl methacrylate (PMMA).

Results and Discussion

XRD patterns of the precursor and those after different milling times are shown in Figure 1. The patterns of the precursor are characteristic of layered double hydroxides as found for pyroaurite ($Mg_6Fe_2(OH)_{16}CO_3{\cdot}4H_2O$; PDF 25-0521) and hydrotalcite ($Mg_6Al_2(OH)_{16}CO_3{\cdot}4H_2O$; PDF 41-1428). After milling the LDH-CO_3 for 5 h the diffraction pattern of the sample consists of broad peaks where their position and intensities suggest the formation of the spinel phase with cubic structure and lattice constant a_0 = 8.381 Å.

The crystallite size, D (nm), and the degree of microstrain, e (arbitrary units), of $CoFe_2O_4$ samples obtained by mechano-chemical milling of iron−cobalt hydroxide carbonates (5, 10, and 15 h of treatment) and of $CoFe_2O_4$ synthesized at 773 K (**TS**) are determined from the experimental XRD profiles (Table 1) using the Scherrer equation. The approach uses the single-line method of analysis, which is based on the assumption that the width broadening is described by a Lorentz function and the microstrain is described by a Gaussian function.[19] The observed diffraction profile is a convolu-

(12) (a) Ding, J.; Miao, W. M.; McCormick, P. G.; Street, R. *Appl. Phys. Lett.* **1994**, *65*, 3135. (b) Ding, J.; McCormick, P. G.; Street, R. *Solid State Commun.* **1995**, *95*, 31. (c) Ding, J.; McCormick, P. G.; Street, R. *J. Magn. Magn. Mater.* **1997**, *171*, 309. (d) Shi, Y.; Ding, J.; Liu, X.; Wang, J. *J. Magn. Magn. Mater.* **1999**, *205*, 249.

(13) Fecht, H. J. *Nanostruct. Mater.* **1995**, *6*, 33.

(14) Ma, E.; Atzmon, M.; Koch, C. C. *2001, Zurich*; Trans Tech Publications: Zurich, 2002.

(15) Suryanarayana, C. *Prog. Mater. Sci*. **2001**, *46*, 1.

(16) (a) Mahmoud, M. H.; Hamdeh, H. H.; Ho, J. C.; O'Shea, M. J.; Walker, J. C. *J. Magn. Magn. Mater.* **2000**, *220*, 139. (b) Druska, P.; Steinike, U.; Šepelák, V. *J. Solid State Chem*. **1999**, *146*, 13. (c) Šepelák, V.; Baabe, D.; Mienert, D.; Litterst, F. J.; Becker, K. D. *Scr. Mater.* **2003**, *48*, 961.

(17) Šepelák, V.; Baabe, D.; Litterst, F. J.; Becker, K. D.; *J. Appl. Phys.* **2000**, *88*, 5884.

(18) (a) Roos, W. *J. Am. Ceram. Soc.* **1980**, *63*, 601. (b) Blaskov, V.; Petkov, V. *J. Magn. Magn. Mater.* **1996**, *162*, 331.

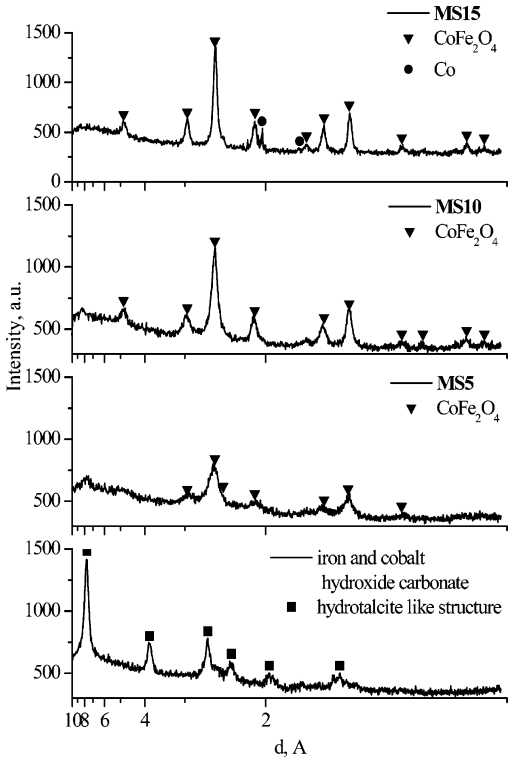

Figure 1. X-ray diffraction patterns (λ = 1.789 Å) of the precursor and the products from the mechano-chemical process as a function of treatment time.

Table 1. Crystallite Size (*D*) and Microstrain (*e*) of Investigated Samples

sample	*D*/nm	$e*10^3$/a.u.
MS5	5.1	12.5
MS10	8.6	5.7
MS15	12.2	3.4
TS	26.5	0.9

tion of the two functions, the so-called Voigt function. In our case, the estimation is made using the most intense reflection of the spectra (d = 2.5310 Å, hkl = 311).

The progression of the diffraction patterns shows two processes are taking place. First, the layered double hydroxide decomposes into the spinel, and second, the spinel reduces partially to cobalt metal after being subjected to an increase in the size of the particles. The increase in size is also evidenced by the reduction of the microstrain that is commonly associated with a diminution of structural defects. It is interesting to note that the process of crystallization continues as a function of treatment time and at later stages is accompanied by the reduction to cobalt. Menzel and co-workers have previously evidenced that high-energy milling of magnesium and nickel ferrite spinels in a steel vial and using steel balls induces the reduction of ferric ions to metallic iron.[20]

Transmission electron microscopy (Figure 2) shows first that the particles tend to agglomerate due to the dipolar field of each particle, and second, the contrast in the fine structures suggest that nanoparticles are

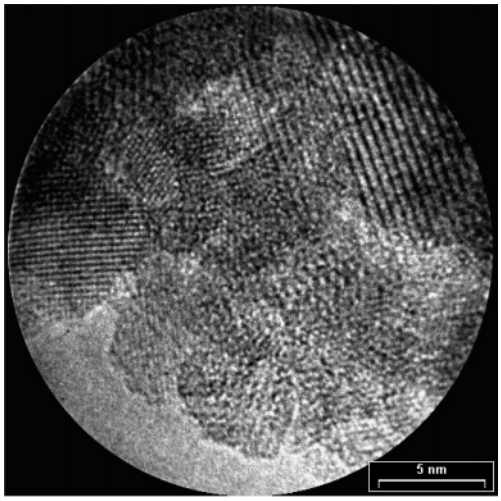

Figure 2. Transmission electron micrograph of the sample **MS5**.

highly crystalline. The agglomeration renders the estimation of the distribution of particle size difficult. The shape of the majority of the particles appears circular. However, due to the contrast we are able to give only average values of the diameter of the particles in the three samples, that is 6, 10, and 14 nm for the 5-, 10-, and 15-h treated samples, respectively.

The infrared spectrum of the precursor shows the characteristic peaks belonging to the carbonate group vibrations (1480 cm^{-1}, 1345 cm^{-1}, 1100 cm^{-1}, 840 cm^{-1}) and those due to M−O stretching mode (350 cm^{-1}) and to M−OH (475 cm^{-1}, 710 cm^{-1}). Spinel structure of iron or cobalt belongs to the $Fd3m$ space group and possesses four IR active vibrational modes.[21] In the IR spectra of the mechanically treated samples the four bands characteristic of a spinel phase are present. The two high-frequency bands (between 550 and 700 cm^{-1} for all the studied samples) are due to vibrations belonging to the octahedral symmetry modes attributable to AOB_3 and BOB_2 stretches of the spinel lattice.[22] In the case of **MS5**, these IR bands are shifted to higher energies compared to those reported in the literature.[23] The IR spectrum of **MS10** displays broad bands, typical for spinel mixed oxides with cationic vacancies.[24] The band observed at 635 cm^{-1} is considered as characteristic for substituted cobalt ferrites with vacancies of ordered type.[24]

To estimate the distribution of the cobalt in the ferrite spinel for the different milling times, ^{57}Fe-Mössbauer spectra were recorded at 295 and 77 K. Figure 3 shows the three room-temperature spectra. The symbols represent the experimental data and the continuous lines correspond to least-squares fits. The calculated spectrum of each individual component (tetrahedral (A site) and octahedral (B site) in different environments) is represented by a continuous line. The best

(19) Koch, C. J. W.; Madsen, M. B.; Morup, S.; Christiansen, G.; Gerward, L.; Villadsen, J. *Clays Clay Miner.* **1986**, *34*, 17.
(20) Menzel, M.; Šepelák, V.; Becker, K. D. *Solid State Ionics* **2001**, *141−142*, 663.
(21) Farmer, V. *Infrared Spectra of Minerals*; Mineralogic Society:, London, 1974.
(22) (a) Ishii, M.; Nakahira, M.; Yamanaka, T. *Solid State Commun.* **1972**, *11*, 209. (b) Busca, G.; Lorenzelli, V.; Escribano, V. *Chem. Mater.* **1992**, *4*, 595.
(23) Uzunova, E.; Klissurski, D.; Mitov, I.; Stefanov, P. *Chem. Mater.* **1993**, *5*, 576.
(24) Gillot, B.; Jemmali, F.; Rousset, A. *J. Solid State Chem.* **1983**, *50*, 138.

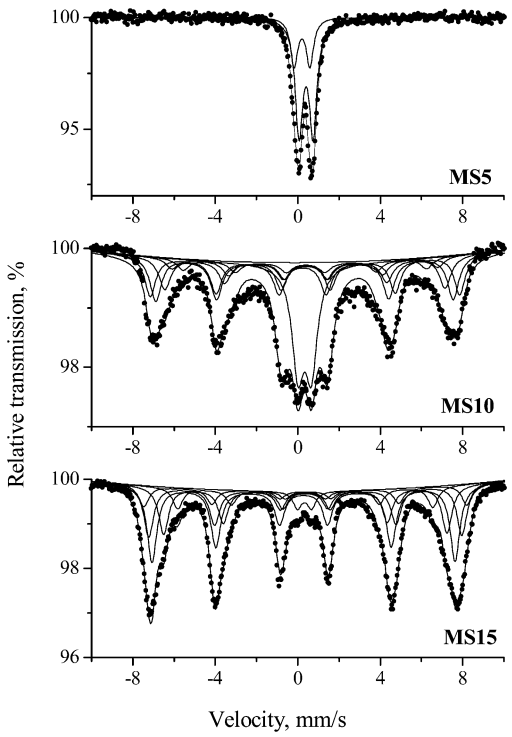

Figure 3. Mössbauer spectra of $CoFe_2O_4$ at 295 K for different milling times; symbols represent the experimental data and the continuous lines correspond to least-squares fits.

Table 2. Mössbauer Parameters of Investigated Samples

sample	components[a]	IS mm/s	QS mm/s	H_{eff} kOe	fwhm mm/s	G %
MS5, 295 K	Db1 Fe^{3+}-$_{tetra}$	0.21	0.77		0.42	28
	Db2 Fe^{3+}-$_{octa}$	0.40	0.68		0.45	72
MS5, 77 K	Sx1 Fe^{3+}-$_{tetra}$	0.30	0.00	485	0.68	28
	Sx2 Fe^{3+}-$_{octa}$	0.40	0.00	508	0.70	29
	Sx3 Fe^{3+}-$_{octa}$	0.40	0.00	457	0.72	19
	Sx4 Fe^{3+}-$_{octa}$	0.40	0.00	425	0.72	11
	Sx5 Fe^{3+}-$_{octa}$	0.40	0.00	377	0.72	9
	Db Fe^{3+}-$_{octa}$	0.39	0.80		0.52	4
MS10, 295 K	Sx1 Fe^{3+}-$_{tetra}$	0.28	0.00	449	0.66	25
	Sx2 Fe^{3+}-$_{octa}$	0.37	0.00	467	0.68	21
	Sx3 Fe^{3+}-$_{octa}$	0.37	0.00	423	0.68	14
	Sx4 Fe^{3+}-$_{octa}$	0.37	0.00	401	0.68	9
	Sx5 Fe^{3+}-$_{octa}$	0.37	0.00	367	0.68	7
	Db Fe^{3+}-$_{octa}$	0.33	0.65		0.71	23
MS10, 77 K	Sx1 Fe^{3+}-$_{tetra}$	0.30	0.00	495	0.45	34
	Sx2 Fe^{3+}-$_{octa}$	0.40	0.00	518	0.49	40
	Sx3 Fe^{3+}-$_{octa}$	0.40	0.00	478	0.49	16
	Sx4 Fe^{3+}-$_{octa}$	0.40	0.00	466	0.49	3
	Sx5 Fe^{3+}-$_{octa}$	0.40	0.00	440	0.49	7
MS15, 295 K	Sx1 Fe^{3+}-$_{tetra}$	0.28	0.00	457	0.57	36
	Sx2 Fe^{3+}-$_{octa}$	0.37	0.00	487	0.57	9
	Sx3 Fe^{3+}-$_{octa}$	0.37	0.00	472	0.57	22
	Sx4 Fe^{3+}-$_{octa}$	0.37	0.00	427	0.57	21
	Sx5 Fe^{3+}-$_{octa}$	0.32	0.00	385	0.57	9
	Db Fe^{3+}-$_{octa}$	0.32	0.65		0.51	3
MS15, 77 K	Sx1 Fe^{3+}-$_{tetra}$	0.25	0.00	496	0.54	38
	Sx2 Fe^{3+}-$_{octa}$	0.36	0.00	524	0.66	21
	Sx3 Fe^{3+}-$_{octa}$	0.36	0.00	518	0.66	16
	Sx4 Fe^{3+}-$_{octa}$	0.36	0.00	509	0.66	13
	Sx5 Fe^{3+}-$_{octa}$	0.36	0.00	478	0.66	12

[a] Sx = sextet; Db = doublet.

parameters of the fits of the Mössbauer spectra are given in Table 2.

The precursor exhibits a quadrupole doublet with IS = 0.34 mm/s, QS = 0.70 mm/s, indicating that the hydroxide-carbonate precursor is paramagnetic and that the iron is in the trivalent state. As shown in Figure 3 the spectrum of **MS5** presents a doublet that can be fitted to two theoretical doublets arising from the two possible iron coordination modes. **MS10** (Figure 3) shows a spectrum consisting of a central doublet (G = 20%) superposed on a sextet pattern (Table 2). This suggests the presence of a distribution of size where the bigger particles have blocking temperature exceeding 295 K. The spectrum of **MS15** (Figure 3) shows a considerable diminution of the doublet component (G = 3%) suggesting the increase in particle size in agreement with the crystallographic and microscopy results.

The Mössbauer spectra of **MS10** and **MS15** exhibit magnetic splitting at RT. It should be noted that acceptable data fitting has been obtained only when the B-site pattern is assumed to be a superposition of more than one sextet. In our case the hyperfine interaction of the B-site can be fitted by up to four overlapping six-line patterns, which agrees with the observations of other authors for ferrite samples.[16a,25] Sawatzky and co-workers interpreted this phenomenon in terms of the random occupancy of the tetrahedral site by Fe^{3+} and Co^{2+}.[25] Consequently, the statistical distribution of Co^{2+} ions at the A-site will result in different nearest neighbors to Fe^{3+} ions in the B-site. The intensities of the four different B-sites are proportional to the probabilities that an Fe^{3+} (B-site) ion has 6Fe, 5Fe1Co, 4Fe2Co and 3Fe3Co nearest neighbors.

The doublets observed in all milled samples arise from Fe in ultradispersed ferrite particles exhibiting superparamagnetic (SPM) behavior.[26] As the SPM relaxation time becomes longer at temperatures below the blocking temperatures the Mössbauer spectra result in the observation of a superposition of sextets. Mössbauer spectra taken below the blocking temperature at 77 K are shown in Figure 4. The hyperfine parameters are given in Table 2. The change in the spectrum on lowering the temperature from 295 to 77 K is typical for SPM materials. This indicates that **MS5** consists of entirely nanometric SPM particles at 295 K and only 5% of them remained unblocked at 77 K. The central doublets present in the spectra of **MS10** and **MS15** at 295 K can be attributed to the fraction of superparamagnetic particles present in the samples. Using the results obtained from Mössbauer spectra, we estimate that the **MS5** sample contains 3% of particles less than 4 nm and 97% in the range 4−10 nm, while for **MS10** 20% of the particles are 4−10 nm and 80% are larger than 10 nm.[27] These estimations are in agreement with the X-ray diffraction results shown in Figure 1. The fraction of SPM particles decreases with increasing time of milling.[28]

The broadening of the lines in the spectrum of **MS10** compared to that of **MS15** indicates the presence of a wide distribution of magnetic fields at the Fe^{3+} nuclei;

(25) Sawatzky, G. A.; Van der Woude, F.; Morrish, A. H. *J. Appl. Phys*. **1968**, *39*, 1024.
(26) (a) Shi, Y.; Ding, J.; Yin, H. *J. Alloys Compd.* **2000**, *308*, 290. (b) Ahn, Y.; Choi, E. J.; Kim, S.; Ok, H. N. *Mater. Lett.* **2001**, *50*, 47.
(27) (a) Panda, R. N.; Gajbhiye, N. S.; Balaji, G. *J. Alloys Compd.* **2001**, *326*, 50. (b) Van der Kraan, A. M. *Phys. Status Soidi A* **1973**, *18*, 215.
(28) (a) Rondinone, A. J.; Samia, A. C. S.; Zhang, Z. J. *J. Phys. Chem. B* **1999**, *103*, 6876. (b) Li, X.; Kutal, Ch. *J. Alloys Compd.* **2003**, *349*, 264.

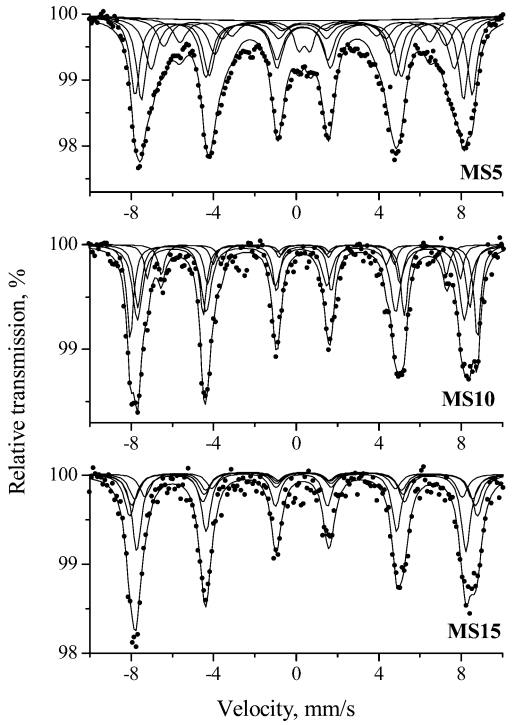

Figure 4. Mössbauer spectra of $CoFe_2O_4$ at 77 K for different milling times; symbols represent the experimental data and the continuous lines correspond to least-squares fits.

Table 3. Cation Distribution Estimated from the Fitted Mössbauer Spectra

sample	calculated formula
MS5, RT	$(Co_{0.44}Fe_{0.56})[Co_{0.56}Fe_{1.44}]O_4$
MS5, LNT	$(Co_{0.42}Fe_{0.58})[Co_{0.58}Fe_{1.42}]O_4$
MS10, RT	$(Co_{0.34}Fe_{0.66})[Co_{0.66}Fe_{1.34}]O_4$
MS10, LNT	$(Co_{0.31}Fe_{0.69})[Co_{0.69}Fe_{1.31}]O_4$
MS15, RT	$(Co_{0.27}Fe_{0.73})[Co_{0.73}Fe_{1.27}]O_4$
MS15, LNT	$(Co_{0.24}Fe_{0.76})[Co_{0.76}Fe_{1.24}]O_4$
TS	$(Co_{0.13}Fe_{0.87})[Co_{0.87}Fe_{1.13}]O_4$

it can be attributed to the nanocrystalline structure with different particle sizes.

Recently accumulated data for a number of spinel ferrites[16a,16c,29] clearly demonstrate that high-energy milling is able to induce redistribution of cations between (A) and [B] sites. In our case, the model used for simulating the Mössbauer spectra permits the calculation of the inversion parameter (the amount of trivalent Fe ions at A-sites). The data obtained for the cation distribution between the (A) and the [B] sites are given in Table 3. It is clear from the table that the degree of inversion in mechano-chemically synthesized cobalt ferrite increases with increasing milling time and approaches that of a thermochemically synthesized one.

Cobalt ferrite bulk material ($CoFe_2O_4$) is known to be a ferrimagnetic oxide that crystallizes with the cubic inverse spinel structure. It has a very high cubic magnetocrystalline anisotropy leading to high theoretical coercivity: 25.2 kOe at 5 K (maximum observed at 2 K is 22 kOe[5]) and 5.4 kOe at 300 K, and a saturation magnetization of 93.9 emu/g at 5 K and 80.8 emu/g at 300 K.[30]

Magnetic properties (isothermal magnetizations and ZFC−FC measurements) of **MS5**, **MS10**, and **MS15** are presented in Figures 5−7, respectively. It is important to note that saturation of the magnetization is never reached (in the magnetic field range explored (±5 T)) for all the samples and measuring temperatures. Given that TEM examinations indicate that these samples contain nearly spherical particles, shape anisotropy is absent and cannot contribute to the magnetic hardness, and consequently saturation is expected in the maximum field used in our experiments. The characteristic parameters are reported in Table 4.

The absence of saturation, coercivity and remanance for **MS5** at 295 K can be explained by a size effect. It is well-known that below a critical size, lowest magnetic energy of a ferromagnetic or ferrimagnetic particle is obtained if all the magnetic moments are parallel. This happens when the particle size gets close to the thickness of the Bloch walls. When such a single domain particle is magnetized in some direction, it does not change its direction because of the barrier due to magnetocrystalline anisotropy energy. According to Stoner and Wohlfarth, the magnetocrystalline anisotropy E_A of a single-domain particle can be approximated as

$$E_A = KV \sin^2\theta \tag{1}$$

where K is the magnetocrystalline anisotropy constant, V is the volume of the nanoparticle, and θ is the angle between the magnetization direction and the easy axis of the nanoparticle. Furthermore, in the case of ultrafine particles this barrier can be less than or comparable to the thermal agitation leading to fluctuations of the global moment of the particles between the easy directions. According to Néel,[31] if an ensemble of such particles is put in a high magnetic field to overcome the dipolar field between particles their moments will line up parallel to the applied field. If the field is switched off, the magnetization should obey the following law:

$$M_r = M_s \exp(-t/\tau) \tag{2}$$

where M_s is the saturation magnetization, t is that time after removal of the magnetic field, and τ is the relaxation time which is thermally activated and given by

$$1/\tau = f_0 \exp(-KV/k_B T) \tag{3}$$

where f_0 is a frequency factor usually taken to be 10^9 sec^{-1},[32] T is the temperature, and k_B is the Boltzmann constant. Consequently, if V is greater than a critical value V_P or T is smaller than the so-called blocking temperature T_B, τ is large compared to the time necessary to measure the magnetization. As the external field is decreased, the magnetic moments do not

(29) (a) Oliver, S. A.; Harris, V. G.; Hamdeh, H. H.; Ho, J. C.; *Appl. Phys. Lett.* **2000**, *76*, 2761. (b) Šepelák, V.; Tkadova, K.; Boldyrev, V. V.; Levissmann, S.; Becker, K. D. *Physica B* **1997**, *234−236*, 617.

(30) (a) Grigova, M.; Blythe, H. J.; Blaskov, V.; Rusanov, V.; Petkov, V.; Masheva, V.; Nihtianova, D.; Martinez, Ll. M.; Muñoz, J. S.; Mikhov, M. *J. Magn. Magn. Mater*. **1998**, *183*, 163. (b) Chinnasamy, C. N.; Jeyadevan, B.; Shioda, K.; Tohji, K.; Djayaprawira, D. J.; Takahashi, M.; Joseyphus, R. J.; Narayanasamy, A. *Appl. Phys. Lett.* **2003**, *83*, 2862.

(31) Herpin, A. *Théorie du Magnétisme*; PUF: Paris, France, 1968.

(32) Jacobs, I. S.; Bean, C. P. In *Magnetism*; Rado, G. T., Suhl, H., Eds.; Academic Press: New York, 1963; vol. 3, p 271.

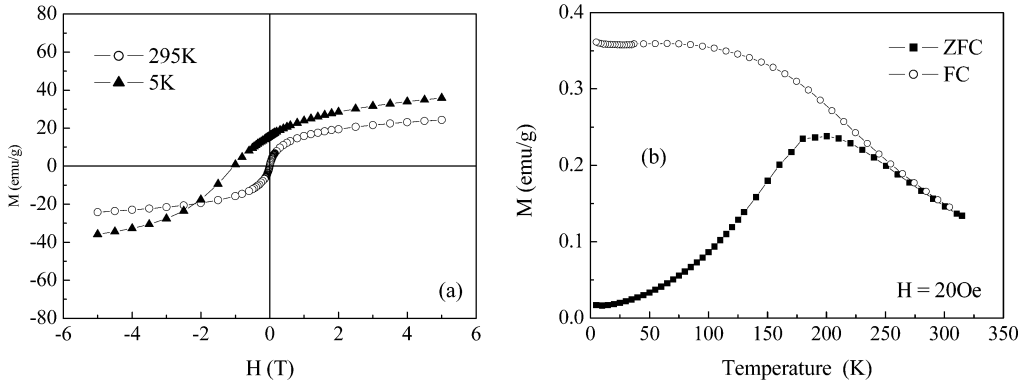

Figure 5. Isothermal magnetization (a) and ZFC−FC measurements (b) of 5-h milled $CoFe_2O_4$.

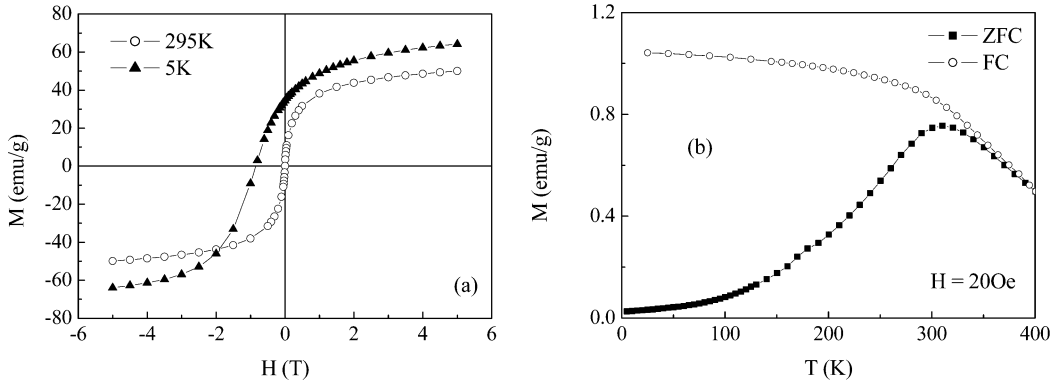

Figure 6. Isothermal magnetization (a) and ZFC−FC measurements (b) of 10-h milled $CoFe_2O_4$.

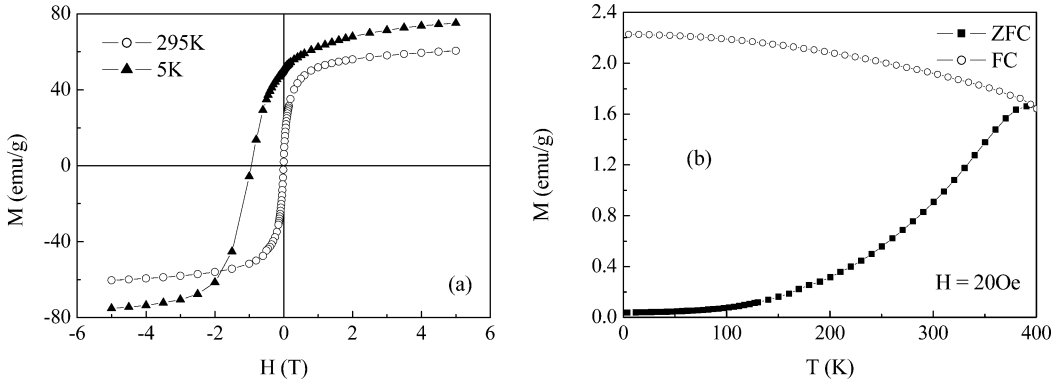

Figure 7. Isothermal magnetization (a) and ZFC−FC measurements (b) of 15-h milled $CoFe_2O_4$.

Table 4. Magnetic Parameters for the $CoFe_2O_4$ Samples

sample	temp. (K)	H_c (T)	M_r (emu/g)	est. M_s (emu/g)	M_r/M_s	T_B (K)
MS5	295	0	0	28.90	0	200
	5	1.040	15.80	43.67	0.36	
MS10	295	0	0	55.85	0	310
	5	0.850	34.50	71.80	0.48	
MS15	295	0.005	2.05	64.70	0.03	390
	5	0.940	50.61	81.17	0.62	

return to random directions, a remnant magnetization subsists in zero field and the magnetization exhibits a hysteresis. In the opposite sense, if V is smaller than V_P or T is higher than T_B, τ becomes small enough for the magnetization to fluctuate during the measurement. The measured average value is zero in zero applied field and an ensemble of such particles behaves in a nonzero field in the same manner as an ensemble of paramagnetic atoms. The phenomenon, called "superparamagnetism", can be described by Langevin's theory of paramagnetism, and the magnetization is given by:[31]

$$\boldsymbol{M}(H,T) = M_s L\left[\frac{M_s VH}{k_B T}\right] \quad (4)$$

where M_s is the saturation magnetization of our sample, L is the Langevin function, V is the volume of the particle, k_B is the Boltzmann constant, T is the temperature, and H is the magnetic field. According to this Langevin function the smaller the particles, the higher is the magnetic field necessary to attain the saturation of the system.

However, saturation magnetization can be estimated[33] from zero extrapolation of M versus $1/H$ and the ratio M_r/M_s can be calculated. It is observed from the estimated values (Table 4) that M_s and M_r/M_s

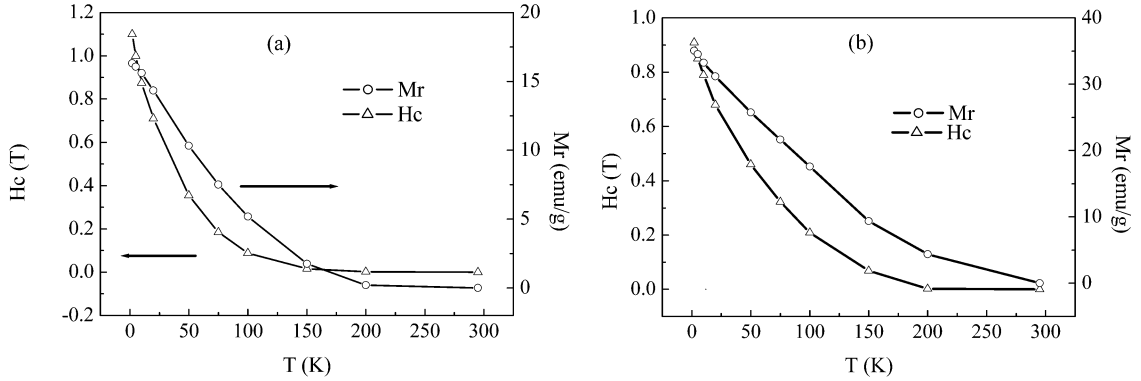

Figure 8. Temperature dependence of the coercive field (H_c) and remanant magnetization of **MS5** (a) and **MS10** (b).

increase with the duration of the mechanical treatment confirming in the increase of the average particles size in agreement with the other physical methods. The known saturation magnetization of the bulk material (see above) is not reached even after 15 h of treatment, indicating that either the objects formed are core/shell particles with spin-glass-like surface layer[33] or that even for such long treatment time some of the ultrafine particles remain. Furthermore, the highest value of the squareness ratio (given by M_r/M_s) for our samples reaches 0.62 indicating that the system consists of randomly oriented equi-axial particles with cubic magnetocrystalline anisotropy,[34] but still this value remains lower than that for bulk materials. We observed that the squareness decreases with milling time (i.e., when the size of the particles increases). Similar tendencies have been reported for $CoFe_2O_4$ of less than 5 nm[35] and γ-Fe_2O_3 (6 nm)[36] and have been attributed to a progressive change of magnetocrystalline anisotropy from cubic to axial structure.

The blocking temperature T_B is often identified with the temperature at which a maximum in the zero-field cooled (ZFC) magnetization curve is observed. T_B can be associated with an average size of the particles. The point at which the ZFC−FC starts to diverge is associated with the blocking temperature of the bigger particles. The difference between these two temperatures reflects the distribution in the particle size. The blocking temperatures for the investigated samples are reported in Table 4. The increase of the particle size is also confirmed by the increase of the blocking temperature with treatment time. According to Liu et al.[2] the blocking temperatures observed could be associated with particles of average size corresponding to 6, 10, and 14 nm. It is well-known that the position of the maximum in the ZFC curves is highly sensitive to the aggregation level of the particles and to the resulting dipolar magnetic interactions between them.[37] However, the values thus-obtained are in good agreement with those determined from TEM and X-ray diffraction. It appears that dipolar interaction, present as an agglomeration of the particles, has little effect on the blocking temperature.

The coercive field H_c is a very important parameter in particulate media for application in magneto-recording. In the low-temperature regime, where the particles are blocked, it is equal to the value expected for single domain.[37] In the case of uniaxial symmetry, the temperature dependence of the coercivity can be formulated by the relation

$$H_c = H_{c0}[1 - \sqrt{(T/T_B)}] \quad (5)$$

And in the case of random distribution of easy axis of the particles this relation becomes

$$H_c = H_{c0}[1 - (T/T_B)] \quad (6)$$

Usually, volume distribution has to be taken into account, leading to the expression

$$H_c = H_{c0}[1 - (T/T_B)^{0.77}] \quad (7)$$

The temperature dependence of the coercive field of **MS5** and **MS10** is reported in Figure 8a and b. Zhang et al.[38] have shown that for 3-nm $CoFe_2O_4$ particles dispersed in polystyrene resin the temperature dependence of H_c varies as $T^{1/2}$ like for noninteracting nanoparticles with uniaxial symmetry. In our case, this variation could neither be simulated with a law in $T^{1/2}$ nor with $T^{0.77}$. The coercive field decreases more rapidly than expected and is better defined by an exponential decay.

We have also carried out measurements for the hysteresis loops at 2 K after either ZFC or FC. For an FC hysteresis loop the sample was first heated to 400 K and then cooled to 2 K in an applied field of 5 T and then the hysteresis loop was measured. The results are reported in Figure 9a and b for **MS5** and **MS10**, respectively. On both graphs a loop shift is observed indicating that H_c for FC is greater than H_c for ZFC. The presence of this loop shift is generally attributed[39] to the presence of core/shell particles where the core is constituted of moments magnetically coupled, while the surface is formed of disordered moments. The existence of a spin-glass shell in ferrite nanoparticle can be rationalized by the broken exchange bonds at its surface. As mentioned previously, the spinel structure

(33) Tung, L. D.; Kolesnicheko, V.; Caruntu, D.; Chou, N. H.; O'Connor, C. J.; Spinu, L. *J. Appl. Phys.* **2003**, *93*, 7486.
(34) Berkowitz, A. E.; Kneller, E. *Magnetism and Metallurgy*: Academic Press: New York, 1969; vol. 1, ch. 8.
(35) Noumen, N.; Pileni, M. P. *J. Phys. Chem.* **1999**, *100*, 1867.
(36) Coey, J. M. D.; Khalafalla, D. *Phys. Status Solidi A* **1972**, *11*, 229.
(37) Dormann, J. L.; Fiorani, D.; Tronc, E. In *Advances in Chemical Physics, Vol. 18*; Prigogine, I., Rice, S. A., Eds.; John Wiley and Sons: New York, 1997.
(38) Zhang, X. X.; Hernandez, J. M.; Tejada, J.; Ziolo, R. F. *Phys. Rev B* **1996**, *54*, 4101.
(39) Muroi, M.; Street, R.; McCormick, P. G.; Amighian, J. *Phys. Rev. B* **2001**, *63*, 184414.

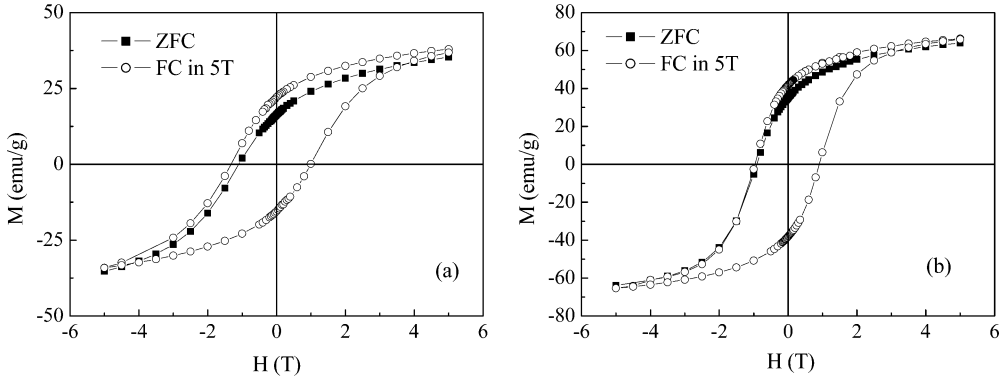

Figure 9. ZFC and FC (5 T) hysteresis loops at 2 K of **MS5** (a) and **MS10** (b).

contains two different cation sites: eight tetrahedral A-sites and sixteen octahedral B-sites. The possible interactions between the different sites are the A−A, B−B, B−A ,and A−B near neighbor interactions. In many spinel ferrites the dominant interaction is A−B, thus the spins on the A and B sites are antiparallel leading to a ferrimagnetic arrangement of moments. This A−B coupling operates via a super-exchange interaction mediated by an intervening oxygen ion. At the surface of the grains, the modification in coordination and bond breaking may result in a distribution of exchange fields as well as spin canting or perturbations in crystal field inducing surface anisotropy. As expected this phenomenon becomes negligible as the particle size is increased (that is, increasing the core-to-surface ratio). Indeed, the differences between the coercive fields ΔH_c are around 0.220 and 0.054 T, respectively, for **MS5** and **MS10**.

Although the blocking temperature is insensitive to the dipolar interactions between particles, the coercive field is more sensitive. One of the reasons for the enhanced coercive field (see Table 4) is believed to be by a dipolar mechanism. The latter is also responsible for the large temperature dependence.

Conclusion

The high-energy ball-milling of the layered iron−cobalt hydroxide carbonates results in the formation of nanocrystalline cobalt ferrite where the particle size can be controlled by the treatment time. All the measurement techniques employed indicate that the particle size increases with the treatment time. The variation of the blocking temperature with grain size has been explained on the basis of finite size effects. The observed hysteresis loop shift (from ZFC to FC) has been attributed to a canting of surface spins. This work shows that nanosize $CoFe_2O_4$ particles can be synthesized by the combination of coprecipitation under ultrasonic treatment and subsequent mechanical milling. This is a promising technique for a relatively large-scale preparation of cobalt ferrite nanoparticles.

Acknowledgment. This work was supported by the Bulgarian Ministry of Education and Science and the French Ministry of Foreign Affairs under the exchange research program RILA (bilateral project Rila11/2003) and by the CNRS-France.

CM049189U